


Toward Heisenberg-Limited Rabi Spectroscopy

Ravid Shaniv, Tom Manovitz, Yotam Shapira, Nitzan Akerman, and Roei Ozeri

Department of Physics of Complex Systems, Weizmann Institute of Science, Rehovot 7610001, Israel

 (Received 29 August 2017; revised manuscript received 25 December 2017; published 14 June 2018)

The use of entangled states was shown to improve the fundamental limits of spectroscopy to beyond the standard-quantum limit. Here, rather than probing the free evolution of the phase of an entangled state with respect to a local oscillator, we probe the evolution of an initially separable two-atom register under an Ising spin Hamiltonian with a transverse field. The resulting correlated spin-rotation spectrum is twice as narrow as that of an uncorrelated rotation. We implement this ideally Heisenberg-limited Rabi spectroscopy scheme on the optical-clock electric-quadrupole transition of $^{88}\text{Sr}^+$ using a two-ion crystal. We further show that depending on the initial state, correlated rotation can occur in two orthogonal subspaces of the full Hilbert space, yielding entanglement-enhanced spectroscopy of either the average transition frequency of the two ions or their difference from the mean frequency. The use of correlated spin rotations can potentially lead to new paths for clock stability improvement.

DOI: [10.1103/PhysRevLett.120.243603](https://doi.org/10.1103/PhysRevLett.120.243603)

Different quantum technologies rely on entangled states as their primary resource. In quantum metrology it was shown that entangled states can reduce the uncertainty in spectroscopy. Spin-squeezed states in atomic ensembles have shown spectroscopic uncertainty below the standard quantum limit (SQL) [1–7]. In the extreme case of fully entangled spins, it was shown that using Ramsey-like spectroscopy of a Greenberger-Horne-Zeilinger state leads to Heisenberg-limited estimation of the transition frequency [8–13].

In Ramsey spectroscopy, the phase of a free-evolving superposition is compared to a local oscillator (LO). Alternatively, in Rabi spectroscopy, the state evolution under a time-dependent Hamiltonian is investigated. Under the rotating-wave approximation, the Rabi Hamiltonian, $H = \hbar[\Omega\sigma_y + \delta\sigma_z]$, generates spin rotations. Here, σ_i are the Pauli spin operators, Ω is the Rabi frequency, and δ is the detuning of the Rabi Hamiltonian from the atomic transition frequency. The initial state is a superposition of the Rabi-Hamiltonian dressed states [14]. The $\delta = 0$ point at which the Rabi Hamiltonian frequency is on resonance is the point at which spin rotation is maximal. The width of the Rabi spectrum is determined by the gap between the two dressed states, namely the Rabi frequency Ω . An inherent difference between Rabi and Ramsey spectroscopy is the line shape width, which is roughly 60% broader for Rabi spectroscopy. Another main difference between the two is that while the Ramsey spectrum exhibits multiple fringes, which usually requires calibration in order to determine the resonance peak, the Rabi spectrum exhibits a single peak. When the spectrum is broad, Rabi spectroscopy yields the spectral structure in a clear and straightforward way.

Heisenberg-limited Ramsey spectroscopy investigates the free evolution of superpositions in entangled subspaces.

By the same token, Heisenberg-limited Rabi spectroscopy can be engineered by investigating rotations of states in these entangled subspaces by many-body spin Hamiltonians [15]. Similarly to single-spin Rabi spectroscopy, the resonance frequency is determined by the maximal rotation angle, and the width of the resonance is given by the gap between the two eigenstates of the Hamiltonian in this subspace.

In this Letter, we show that an Ising spin-interaction Hamiltonian with a transverse field generates rotations in two orthogonal subspaces of a two-spin Hilbert space—the even- and odd-parity subspaces. In the even subspace, spanned by $\{|\uparrow\uparrow\rangle, |\downarrow\downarrow\rangle\}$, this Hamiltonian results in Heisenberg-limited Rabi spectroscopy of the average spin transition frequency; whereas in the odd subspace spanned by $\{|\downarrow\uparrow\rangle, |\uparrow\downarrow\rangle\}$, Heisenberg-limited Rabi spectroscopy of the spin’s frequency difference from the mean transition frequency is performed. We implement this protocol using the optical clock electric-quadrupole transition in a two- $^{88}\text{Sr}^+$ -ion crystal and show that the resulting correlated spin rotation spectra are indeed twice as narrow as single-ion Rabi spectra.

Heisenberg-limited spectroscopy was shown to exhibit limited improvement of spectroscopic precision after long averaging times, because as the sensitivity to the resonance frequency increases, so does the sensitivity to dephasing [16]. Theoretical investigations have shown that an improvement of measurement precision or clock stability is possible; however, it depends on the details of the noise and the spectroscopic method. [17,18]. Hence, new Heisenberg-limited spectroscopy technique development can potentially introduce clock stability improvement under different conditions. For short averaging times where projection noise is dominant, Heisenberg-limited

spectroscopy is advantageous, since it yields lower uncertainty for a given integration time.

We investigate a system of two interacting spins, under the influence of an Ising two-spin Hamiltonian with a transverse field:

$$H = \hbar[\Omega\sigma_y \otimes \sigma_y + \delta_1(\sigma_z \otimes I + I \otimes \sigma_z) + \delta_2(\sigma_z \otimes I - I \otimes \sigma_z)]. \quad (1)$$

Here the $\delta_1(\sigma_z \otimes I + I \otimes \sigma_z)$ term represents a magnetic field along the z axis common to both spins, and the term $\delta_2(\sigma_z \otimes I - I \otimes \sigma_z)$ represents the difference between the fields on each spin. The $\Omega\sigma_y \otimes \sigma_y$ term is an Ising-type interaction which creates a correlated rotation of the two spins.

The Hamiltonian in Eq. (1) commutes with $\sigma_z \otimes \sigma_z$ and therefore conserves state parity and does not mix between the even $\{|\downarrow\downarrow\rangle, |\uparrow\uparrow\rangle\}$ and odd $\{|\downarrow\uparrow\rangle, |\uparrow\downarrow\rangle\}$ parity subspaces. In addition, the even and odd subspaces are degenerate under the operations $\sigma_z \otimes I - I \otimes \sigma_z$ and $\sigma_z \otimes I + I \otimes \sigma_z$, respectively. As a result, superpositions of the states $|\uparrow\uparrow\rangle, |\downarrow\downarrow\rangle$ ($|\downarrow\uparrow\rangle, |\uparrow\downarrow\rangle$) are invariant to changes in δ_2 (δ_1).

The two subspaces above can be thought of as two super-spin-half metrological subspaces. As an example, in the even subspace, the two basis states of a super-spin-half system are $|\tilde{\uparrow}\rangle := |\uparrow\uparrow\rangle, |\tilde{\downarrow}\rangle := |\downarrow\downarrow\rangle$. Ising coupling acts as a y rotation in this subspace, $\tilde{\sigma}_y = \sigma_y \otimes \sigma_y$, and a z rotation is generated by $\tilde{\sigma}_z = (\sigma_z \otimes I + I \otimes \sigma_z)$. Rotations around z in the odd subspace are generated by $(\sigma_z \otimes I - I \otimes \sigma_z)$. The Ising Hamiltonian in Eq. (1) therefore performs Rabi spectroscopy in the two spin subspaces with a Rabi frequency Ω and detunings of $2\delta_1$ and $2\delta_2$. The factor of 2 in the detuning results in a twofold narrowing of the Rabi resonance, leading to Heisenberg-limited determination of the resonance frequency under spin projection noise. Notice that a general two-spin state is a direct sum of states in these two subspaces. A measurement will therefore lead to a single bit of spectroscopic information, thus increasing the standard deviation due to projection noise.

In our experiment, the pseudospin states are the two optical-clock transition levels, $5S_{j=\frac{1}{2}, m_j=-\frac{1}{2}}$ and $4D_{j=\frac{3}{2}, m_j=-\frac{3}{2}}$, in trapped $^{88}\text{Sr}^+$ ions. Our ions are trapped in a linear Paul trap and laser-cooled to the ground state of motion [19–21] in the axial direction. We drive the optical clock transition using a 674 nm narrow-linewidth laser (< 50 Hz). We address the two ion crystal with a single large-waist beam which implements both global rotations as well as the transverse Ising Hamiltonian. Alternatively, we individually address a single ion of our choice using a tightly focused laser beam. The state of our ion is detected using state-selective fluorescence detection. For more details about the system, see Refs. [20–22].

The Ising Hamiltonian in Eq. (1) is realized using a Mølmer-Sørensen (MS) interaction [23]. We denote the clock transition carrier frequencies of ion 1 and ion 2 as ω_0^1 and ω_0^2 , respectively. The ions are illuminated with a bichromatic 674 nm laser beam at frequencies

$$\omega_{\pm} = \omega_0 \pm \nu \pm \varepsilon - \delta, \quad (2)$$

where $\omega_0 = (\omega_0^1 + \omega_0^2/2)$ is the average clock transition carrier frequency, ν is the axial trap frequency, ε is a symmetric detuning, and δ is an asymmetric detuning from the sideband transitions. [The name symmetric (antisymmetric) detuning reflects the fact that the detuning of ω_+ and ω_- from the blue and red motional sidebands, respectively, has the opposite (same) sign; see Fig. 1(c).] We also define the center laser frequency as $\omega_L = (\omega_+ + \omega_-/2) = \omega_0 - \delta$. Here, we work in the regime

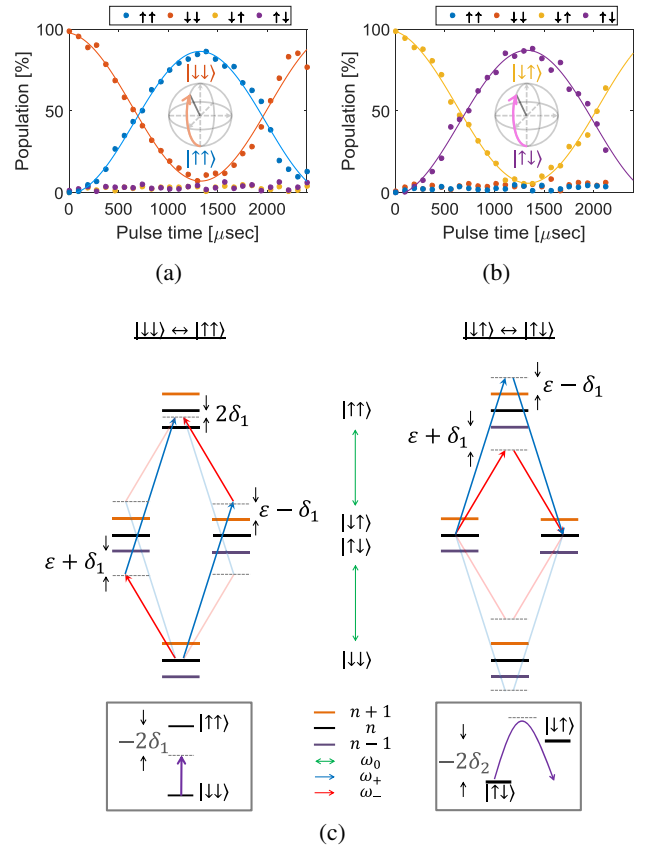


FIG. 1. Coupling in the two metrological subspaces using Mølmer-Sørensen interaction. (a), (b) Experimental results of resonant Rabi nutation between $|\downarrow\downarrow\rangle \leftrightarrow |\uparrow\uparrow\rangle$ and $|\uparrow\downarrow\rangle \leftrightarrow |\downarrow\uparrow\rangle$, respectively. Inset: Rotations illustrated on a Bloch sphere representing each subspace. (c) Laser frequencies and motion energy levels coupled by the Mølmer-Sørensen operation for both the $|\downarrow\downarrow\rangle \leftrightarrow |\uparrow\uparrow\rangle$ (left) and $|\uparrow\downarrow\rangle \leftrightarrow |\downarrow\uparrow\rangle$ (right) transitions. In the limit of large ε , this operation approximates the Hamiltonian H in Eq. (1). Insets: A diagrammatic representation of δ_1 and δ_2 scans in the two subspaces.

$\varepsilon \gg \eta\tilde{\Omega}$, where η is the Lamb-Dicke parameter of the trap axial center-of-mass mode and $\tilde{\Omega}$ is the clock transition Rabi frequency. In this regime, the coupling to motion through the red and blue sidebands can be adiabatically eliminated. In this case, two-photon coupling yields collective spin rotations, and the Hamiltonian is well approximated as an Ising $\sigma_y \otimes \sigma_y$ interaction, with a z transverse field due to $\delta_1 = \delta$. If $\omega_0^1 \neq \omega_0^2$, then dynamics is governed by the Hamiltonian in Eq. (1), where δ_2 represents the difference in detuning between ions and $\Omega = (\eta^2\tilde{\Omega}^2/\varepsilon)$ is the two-spin coupling. Using the notation above, $\delta_1 = \omega_L - \omega_0$ and $\delta_2 = (\omega_0^1 - \omega_0^2/2)$. The insets in Fig. 1(c) show a diagrammatic illustration of the different detunings in this regime. We begin by performing correlated Rabi nutation in the two subspaces using resonant Ising interaction. Here, we have initialized our system in $|\downarrow\downarrow\rangle$ or $|\downarrow\uparrow\rangle$ and turned on our MS interaction, setting $\delta_1 \simeq \delta_2 \simeq 0$. Correlated Rabi nutation curves in the two subspaces are shown in Figs. 1(a) and 1(b). As seen, coupling to states outside the subspace is minimized by the choice of large ε . We observe a complete correlated spin-flip at a π -time of $\tau_\pi = (\pi/\Omega)$, which is about 1300 μs in this experiment.

Next, we performed a wide Rabi spectroscopy scan by scanning δ_1 from $-\varepsilon$ to ε , i.e., nearly to the motional sideband, by scanning the MS laser center frequency, ω_L . A measurement of the populations of the relevant spin states vs δ_1 is shown in Fig. 2. Here we set $\delta_2 \simeq 0$ and the pulse time to τ_π . As seen, when the system is initialized in the even subspace, correlated spin rotation does not occur unless $\delta_1 \simeq 0$. Around this resonant value, marked by a grey background, a sharp $|\downarrow\downarrow\rangle \rightarrow |\uparrow\uparrow\rangle$ transition is observed. This correlated spin-flip resonance is enlarged in the inset of Fig. 2(b). On the other hand, when the system is initialized in the odd subspace, correlated spin-flip occurs at any value of δ_1 . This is due to the fact that the $\{|\downarrow\uparrow\rangle|\uparrow\downarrow\rangle\}$ subspace is insensitive to δ_1 . This odd subspace has been used before as a decoherence-free subspace due to this resilience to common phase noise. In both subspaces, as δ_1 approaches ε , single-photon sideband transitions occur, resulting in rapid population oscillations. We next turned to a combined scan of both δ_1 and δ_2 . This scan was carried out by light-shifting the resonance frequency of only one of the ions using an off-resonance single-addressing beam (see Supplemental Material [24]). With a detuning $\delta_{1s}/2\pi \simeq 3.5$ MHz and a Rabi frequency which varied within the range $\Omega_{1s}/2\pi \simeq 0\text{--}40$ kHz, we scanned the light shift at $\Delta f_{1s}/2\pi \simeq (\Omega_{1s}^2/2\pi\delta_{1s}) \simeq 0\text{--}400$ Hz. By definition, $\delta_2 = \pm \frac{1}{2}\Delta_{1s}/2\pi$. The sign is determined by the specific ion being light-shifted. The magnitude of Δf_{1s} , and therefore δ_2 , was scanned by varying the intensity of the individual addressing laser. For every value of Δf_{1s} a full scan of ω_L was carried out, by changing the parameter δ in Eq. (2). Figure 4 shows the

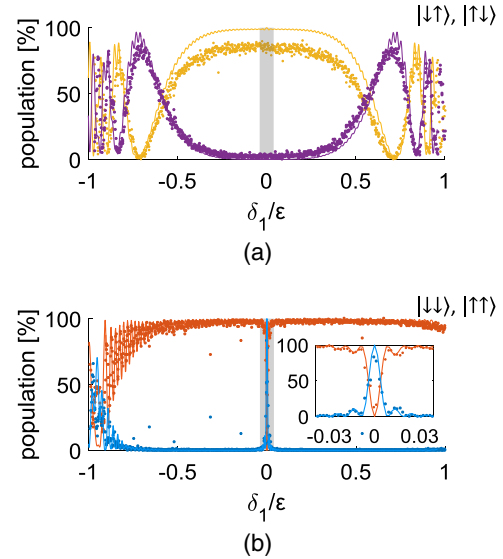


FIG. 2. Broad scan of δ_1 in both subspaces. (a) δ_1 scan results when initializing in $|\downarrow\uparrow\rangle$ and measuring the population in $|\uparrow\downarrow\rangle$ (yellow) and $|\downarrow\uparrow\rangle$ (purple). (b) δ_1 scan results when initializing in $|\downarrow\downarrow\rangle$ and measuring the population in $|\uparrow\uparrow\rangle$ (blue) and $|\downarrow\downarrow\rangle$ (orange). The data were shifted to be symmetric around $\delta_1 = 0$, and the solid lines are simulation results with no fit parameters. The discrepancy between simulation and data in (a) is due to population leaking to $|\downarrow\downarrow\rangle, |\uparrow\uparrow\rangle$ owing to experimental imperfections. The inset of (b) is a magnification of the shaded area in (b). The δ_1/ε interval is shaded in (a) for comparison. In both measurements, $\varepsilon = 2\pi \times 25.5 \text{ kHz} \approx 10\eta\Omega$.

population of spin states $|\uparrow\uparrow\rangle$ and $|\uparrow\downarrow\rangle$ for such a scan, when initializing in $|\downarrow\downarrow\rangle$ and in $|\downarrow\uparrow\rangle$, respectively. As seen, in the odd subspace, a change to Δf_{1s} causes a resonant response every time $\delta_2 = 0$, whereas a change of ω_L does not change the position of this resonance. In the even subspace, a scan of ω_L yields a resonant response whenever $\omega_L - \omega_0 = 0$. The change of Δf_{1s} shifts the position of this resonance symmetrically with respect to the sign of Δf_{1s} , leading to the curved shape in Fig. 3(a). This symmetry proves that in the even subspace, it is only the contribution of Δf_{1s} to δ_1 which changes the resonance position (see Supplemental Material [24]). Note that since symmetric phase noise is more common in our experiment than differential phase noise between the two ions, the resonance in the even subspace is much noisier than that in the odd subspace.

Finally, to determine whether our spectroscopy is Heisenberg limited, we performed a narrower scan of δ_1 and δ_2 , each in its corresponding subspace, and compared the resulting spectrum to that of standard Rabi spectroscopy having the same pulse time τ and the same overall interrogation time. First, we demonstrate spectral width narrowing. Ten short frequency scans of 50 experimental realizations per frequency were recorded, in order to avoid slow frequency drift during each scan. Scans were interlaced between uncorrelated and correlated two-ion Rabi

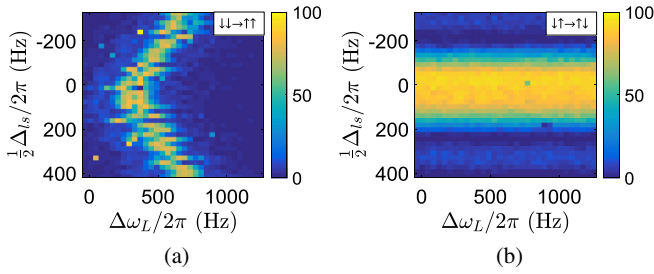


FIG. 3. Sensitivity of correlated rotations to δ_1 and δ_2 . (a) Population of $|\uparrow\uparrow\rangle$ when initializing in $|\downarrow\downarrow\rangle$. (b) Population of $|\uparrow\downarrow\rangle$ when initializing in $|\downarrow\uparrow\rangle$. We shift the resonance frequency of one of the two ions by Δf_{ls} using a tightly focused, off-resonance laser beam. As a result, δ_1 is shifted by $|(\Delta f_{\text{ls}}/2)|$ and δ_2 is shifted by $\pm(\Delta f_{\text{ls}}/2)$, where the sign depends on which ion is shifted. For each value of Δf_{ls} we scan the laser frequency ω_L with respect to an arbitrary offset and measure populations. As shown, a resonance in the odd subspace appears every time $\delta_2 = 0$ regardless of ω_L , which only shifts δ_1 . On the other hand, in the even subspace, Δf_{ls} shifts the δ_1 resonance symmetrically when either of the ions is light-shifted, indicating that the associated change in δ_2 does not affect this subspace. The full two-spin-state populations corresponding to this experiment can be found in the Supplemental Material [24].

spectroscopy. These spectra were shifted to be centered at the same resonance frequency and fitted together to the theory. Here the δ_1 scan in the even subspace was performed by scanning ω_L , and the δ_2 scan in the odd subspace was achieved by scanning Δf_{ls} . Uncorrelated Rabi spectroscopy was performed by a regular single-ion Rabi spectroscopy scan. The spectral shape of the excited-state population in two-level Rabi spectroscopy is [25]

$$P(\uparrow) = A \frac{\sin^2\left(\frac{\Omega t}{2} \sqrt{1 + \left(\frac{\alpha\delta}{\Omega}\right)^2}\right)}{1 + \left(\frac{\alpha\delta}{\Omega}\right)^2}, \quad (3)$$

where Ω is the Rabi frequency, and the contrast parameter A accounts for experimental imperfections. α is the narrowing factor, which is 1 for an uncorrelated Rabi spectroscopy and 2 for perfect two-qubit correlated Heisenberg-limited Rabi spectroscopy. The results of the different scans are shown in Fig. 4. For the δ_1 scan in the even subspace, we obtained $\alpha = 1.92 \pm 0.02$ for a correlated rotation and $\alpha = 1.01 \pm 0.01$ for the single-ion case using a maximum-likelihood fit to Eq. (3). In the odd subspace, a δ_2 scan yielded $\alpha = 1.78 \pm 0.03$ for the correlated case and $\alpha = 0.88 \pm 0.02$ for single-ion spectroscopy. Both odd and even subspaces exhibit correlated rotation spectrum narrowing by a factor close to 2. The insets of Fig. 4 compare uncorrelated and correlated two-ion spectra having the same integration times. The uncorrelated spectrum is the widest, but it holds two data points for each scanned parameter value. Therefore, estimation of the resonance can

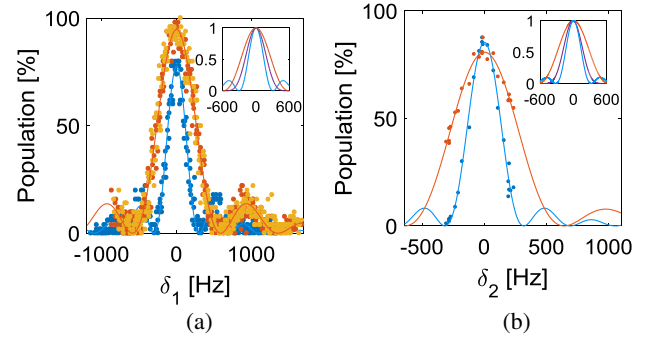


FIG. 4. Heisenberg-limited spectroscopy. (a) Comparison between the δ_1 spectra for the cases of a single ion (red and orange full circles for the right and left ion, respectively) and of two ions correlated by spectroscopy in the even subspace (blue full circles). All spectra are shifted to center around $\delta_1 = 0$ due to small shifts (tens of hertz) and fitted to Eq. (3) (solid blue line). (b) Comparison between the δ_2 spectra of two ions in an uncorrelated (red full circles) and a correlated (blue full circles) measurement in the odd subspace. In the uncorrelated case, the average frequency of the two ions was measured on each ion separately as a function of δ_2 , and both populations were averaged to give the measurement result (See Supplemental Material [24]). The spectra were also shifted to be centered at $\delta_2 = 0$. Insets: Comparison between the normalized uncorrelated case fit, the product of the two single-ion fits in the uncorrelated case, and the normalized correlated fit for both δ_1 and δ_2 scans (red, purple, and blue solid lines, respectively).

be performed with $\sqrt{2}$ reduction in the uncertainty. This reduction can be manifested spectrumwise in a spectrum of the probability of both ions excited. The resulting spectrum is $\sqrt{2}$ narrower than a single-ion case, thus matching the above frequency uncertainty. The correlated case exhibits nearly twice as narrow a spectrum with the same number of experimental realizations.

To demonstrate the estimation of the resonance frequency below the SQL, we analyzed a single even-subspace scan out of the ten presented in Fig. 4. We obtained sensitivities of $0.23 \text{ Hz}/\sqrt{\text{Hz}}$ and $0.43 \text{ Hz}/\sqrt{\text{Hz}}$ for the two-ion correlated and uncorrelated cases, respectively, showing an improvement by a factor of 1.87, well above the expected SQL of $\sqrt{2} \approx 1.41$. This proves that correlated rotation results are indeed well below the standard quantum limit and close to the Heisenberg limit.

In this Letter, only a two-ion crystal was used for a proof-of-principle experiment, and hence the correlated two-ion Rabi spectroscopy yields uncertainty only slightly better compared to a single-ion Ramsey spectroscopy, due to the constant factor in the linewidth of the two methods. However, the features demonstrated here are general and will apply to a larger number of spins as well. For $N \geq 3$ spins, the scaling already wins over the above linewidth factor. The required generalized Hamiltonian that will generate correlated N -spin rotations will be given by

$$\hbar \left(\Omega(\sigma_y)^{\otimes N} + \sum_{i=1}^N \delta_i I \otimes \dots \otimes \sigma_z^i \otimes \dots \otimes I \right). \quad (4)$$

Using this Hamiltonian, an N -fold narrower Rabi spectrum can be measured around the average resonance frequency. The simulation of the above N -body correlated Hamiltonian was proposed in Refs. [26,27]. In principle, a universal quantum simulator can be used to implement multi-ion Heisenberg-limited Rabi spectroscopy on any number of spins.

To conclude, in this Letter we presented and demonstrated a two-ion Heisenberg-limited Rabi spectroscopy. We initialized the ions in a separable state, and by operating with an entangling operator we obtained a spectrum narrower by a factor of $\simeq 2$ with respect to conventional single-ion Rabi spectroscopy. We observed that under the influence of an Ising Hamiltonian, the two-ion system splits into two orthogonal subspaces that can be used as different probes for the difference and the average of the ions' optical resonance frequency, each of them with Heisenberg-limited uncertainty. We believe that the experiment presented here can be scaled up to more than a two-ion crystal, and may be useful as a spectroscopic tool for optical frequency measurements.

This work was supported by the Crown Photonics Center, the ICore-Israeli Excellence Center Circle of Light, the Israeli Science Foundation, the Israeli Ministry of Science Technology and Space, the Minerva Stiftung, and the European Research Council (Consolidator Grant No. 616919-Ionology).

R. S. and T. M. contributed equally to this work.

-
- [1] D. J. Wineland, J. J. Bollinger, W. M. Itano, and D. J. Heinzen, Squeezed atomic states and projection noise in spectroscopy, *Phys. Rev. A* **50**, 67 (1994).
- [2] P. Bouyer and M. A. Kasevich, Heisenberg-limited spectroscopy with degenerate Bose-Einstein gases, *Phys. Rev. A* **56**, R1083 (1997).
- [3] C. Gross, T. Zibold, E. Nicklas, J. Estève, and M. K. Oberthaler, Nonlinear atom interferometer surpasses classical precision limit, *Nature (London)* **464**, 1165 (2010).
- [4] V. Meyer, M. A. Rowe, D. Kielpinski, C. A. Sackett, W. M. Itano, C. Monroe, and D. J. Wineland, Experimental Demonstration of Entanglement-Enhanced Rotation Angle Estimation Using Trapped Ions, *Phys. Rev. Lett.* **86**, 5870 (2001).
- [5] A. Louchet-Chauvet, J. Appel, J. J. Renema, D. Oblak, N. Kjaergaard, and E. S. Polzik, Entanglement-assisted atomic clock beyond the projection noise limit, *New J. Phys.* **12**, 065032 (2010).
- [6] J. G. Bohnet, B. C. Sawyer, J. W. Britton, M. L. Wall, A. M. Rey, M. Foss-Feig, and J. J. Bollinger, Quantum spin dynamics and entanglement generation with hundreds of trapped ions, *Science* **352**, 1297 (2016).
- [7] L. Pezzè, A. Smerzi, M. K. Oberthaler, R. Schmied, and P. Treutlein, Quantum metrology with nonclassical states of atomic ensembles, [arXiv:1609.01609](https://arxiv.org/abs/1609.01609).
- [8] J. J. Bollinger, W. M. Itano, D. J. Wineland, and D. J. Heinzen, Optimal frequency measurements with maximally correlated states, *Phys. Rev. A* **54**, R4649 (1996).
- [9] C. A. Sackett, D. Kielpinski, B. E. King, C. Langer, V. Meyer, C. J. Myatt, M. Rowe, Q. A. Turchette, W. M. Itano, D. J. Wineland, and C. Monroe, Experimental entanglement of four particles, *Nature (London)* **404**, 256 (2000).
- [10] D. Leibfried, B. DeMarco, V. Meyer, D. Lucas, M. Barrett, J. Britton, W. M. Itano, B. Jelenković, C. Langer, T. Rosenband, and D. J. Wineland, Experimental demonstration of a robust, high-fidelity geometric two ion-qubit phase gate, *Nature (London)* **422**, 412 (2003).
- [11] D. Leibfried, M. D. Barrett, T. Schaetz, J. Britton, J. Chiaverini, W. M. Itano, J. D. Jost, C. Langer, and D. J. Wineland, Toward Heisenberg-limited spectroscopy with multiparticle entangled states, *Science* **304**, 1476 (2004).
- [12] D. Leibfried, E. Knill, S. Seidelin, J. Britton, R. B. Blakestad, J. Chiaverini, D. B. Hume, W. M. Itano, J. D. Jost, C. Langer, R. Ozeri, R. Reichle, and D. J. Wineland, Creation of a six-atom "Schrödinger cat" state, *Nature (London)* **438**, 639 (2005).
- [13] T. Monz, P. Schindler, J. T. Barreiro, M. Chwalla, D. Nigg, W. A. Coish, M. Harlander, W. Haensel, M. Hennrich, and R. Blatt, 14-Qubit Entanglement: Creation and Coherence, *Phys. Rev. Lett.* **106**, 130506 (2011).
- [14] C. Cohen-Tannoudji, J. Dupont-Roc, and G. Grynberg, *Atom-Photon Interactions: Basic Processes and Applications* (Wiley, New York, 1992).
- [15] R. Ozeri, Heisenberg limited metrology using quantum error-correction codes, [arXiv:1310.3432](https://arxiv.org/abs/1310.3432).
- [16] S. F. Huelga, C. Macchiavello, T. Pellizzari, A. K. Ekert, M. B. Plenio, and J. I. Cirac, Improvement of Frequency Standards with Quantum Entanglement, *Phys. Rev. Lett.* **79**, 3865 (1997).
- [17] R. Demkowicz-Dobrzanski, J. Kolodynski, and M. Guta, The elusive Heisenberg limit in quantum enhanced metrology, *Nat. Commun.* **3**, 1063 (2012).
- [18] I. D. Leroux, N. Scharnhorst, S. Hannig, J. Kramer, L. Pelzer, M. Stepanova, and P. O. Schmidt, On-line estimation of local oscillator noise and optimisation of servo parameters in atomic clocks, *Metrologia* **54**, 307 (2017).
- [19] D. J. Wineland, C. Monroe, W. M. Itano, D. Leibfried, B. E. King, and D. M. Meekhof, Experimental issues in coherent quantum-state manipulation of trapped atomic ions, *J. Res. Natl. Inst. Stand. Technol.* **103**, 259 (1998).
- [20] N. Akerman, Y. Glickman, S. Kotler, A. Keselman, and R. Ozeri, Quantum control of $^{88}\text{Sr}^+$ in a miniature linear Paul trap, *Appl. Phys. B* **107**, 1167 (2012).
- [21] N. Akerman, N. Navon, S. Kotler, Y. Glickman, and R. Ozeri, Universal gate-set for trapped-ion qubits using a narrow linewidth diode laser, *New J. Phys.* **17**, 113060 (2015).
- [22] T. Manovitz, Individual addressing and imaging of ion in a Paul trap, MSc thesis, Feinberg Graduate School, Weizmann, 2016, <https://www.weizmann.ac.il/complex/>

- [ozeri/sites/complex.ozeri/files/uploads/thesis_submission.pdf](#)
- [23] A. Sorensen and K. Molmer, Entanglement and quantum computation with ions in thermal motion, *Phys. Rev. A* **62**, 022311 (2000).
- [24] See Supplemental Material at <http://link.aps.org/supplemental/10.1103/PhysRevLett.120.243603> for apparatus description and single addressing light shift operation details.
- [25] L. Allen and J. H. Eberly, *Optical Resonance and Two-Level Systems* (John Wiley & Sons, New York, 1975).
- [26] M. Mueller, K. Hammerer, Y. L. Zhou, C. F. Roos, and P. Zoller, Simulating open quantum systems: From many-body interactions to stabilizer pumping, *New J. Phys.* **13**, 085007 (2011).
- [27] A. Bermudez, D. Porras, and M. A. Martin-Delgado, Competing many-body interactions in systems of trapped ions, *Phys. Rev. A* **79**, 060303 (2009).